AGU PUBLICATIONS

JGR

Journal of Geophysical Research: Space Physics

RESEARCH ARTICLE
10.1002/2013JA019284

Key Points:
- Record large-amplitude ELF waves
- MS waves lead to whistler mode growth
- Waves due to injection of plasmaspheric protons at local midnight

Correspondence to:
B. T. Tsurutani,
bruce.t.tsurutani@jpl.nasa.gov

Citation:
Tsurutani, B. T., B. J. Falkowski, J. S. Pickett, O. P. Verkhoglyadova, O. Santolik, and G. S. Lakhina (2014), Extremely intense ELF magnetosonic waves: A survey of polar observations, *J. Geophys. Res. Space Physics*, *119*, 964–977, doi:10.1002/2013JA019284.

Received 6 AUG 2013
Accepted 15 JAN 2014
Accepted article online 22 JAN 2014
Published online 12 FEB 2014

Extremely intense ELF magnetosonic waves: A survey of polar observations

Bruce T. Tsurutani[1], Barbara J. Falkowski[1,2], Jolene S. Pickett[3], Olga P. Verkhoglyadova[1,4], Ondrej Santolik[5,6], and Gurbax S. Lakhina[7]

[1]Jet Propulsion Laboratory, California Institute of Technology, Pasadena, California, USA, [2]Physics and Astronomy Departments, Glendale Community City College, Glendale, California, USA, [3]Physics and Astronomy, University of Iowa, Iowa City, Iowa, USA, [4]CSPAR, University of Alabama in Huntsville, Huntsville, Alabama, USA, [5]Institute of Atmospheric Physics, ASCR, Prague, Czech Republic, [6]Faculty of Mathematics and Physics, Charles University, Prague, Czech Republic, [7]Indian Institute of Geomagnetism, Navi Mumbai, India

Abstract A Polar magnetosonic wave (MSW) study was conducted using 1 year of 1996–1997 data (during solar minimum). Waves at and inside the plasmasphere were detected at all local times with a slight preference for occurrence in the midnight-postmidnight sector. Wave occurrence (and intensities) peaked within~±5° of the magnetic equator, with half maxima at ~±10°. However, MSWs were also detected as far from the equator as +20° and 60° MLAT but with lower intensities. An extreme MSW intensity event of amplitude B_w = ~± 1 nT and E_w = ~± 25 mV/m was detected. This event occurred near local midnight, at the plasmapause, at the magnetic equator, during an intense substorm event, e.g., a perfect occurrence. These results support the idea of generation by protons injected from the plasma sheet into the midnight sector magnetosphere by substorm electric fields. MSWs were also detected near noon (1259 MLT) during relative geomagnetic quiet (low AE). A possible generation mechanism is a recovering/expanding plasmasphere engulfing preexisting energetic ions, in turn leading to ion instability. The wave magnetic field components are aligned along the ambient magnetic field direction, with the wave electric components orthogonal, indicating linear wave polarization. The MSW amplitudes decreased at locations further from the magnetic equator, while transverse whistler mode wave amplitudes (hiss) increased. We argue that intense MSWs are always present somewhere in the magnetosphere during strong substorm/convection events. We thus suggest that modelers use dynamic particle tracing codes and the maximum (rather than average) wave amplitudes to simulate wave-particle interactions.

1. Introduction

Intense ELF magnetosonic waves have been detected at and near the plasmapause [*Russell et al*., 1970; *Gurnett*, 1976; *Perraut et al*., 1982; *Olsen et al*., 1987; *Boardsen et al*., 1992; *Kasahara et al*., 1994; *Horne et al*., 2000; *Andre et al*., 2002; *Santolik et al*., 2002, 2004; *Nemec et al*., 2005, 2006, 2013; *Meredith et al*., 2008; *Pokhotelov et al*., 2008] by a variety of researchers using many different spacecraft. Initial observations indicated that these waves are narrowly confined close to the magnetic equator (within ~2°) and occur at frequencies between twice the proton gyrofrequency and half the lower hybrid resonant frequency. They propagate within ~1° perpendicular to the ambient magnetic field. *Russell et al*. [1970] using OGO 3 plasma wave data noted that the waves will be resonant with the harmonics of the electron bounce frequency and thus could cause pitch angle diffusion of electrons mirroring near the equator. *Gurnett* [1976] analyzing the IMP 6 and Hawkeye 1 data noted that this equatorial noise consisted of a number of harmonically spaced lines and thus suggested that these waves may be interacting with protons, alpha particles, and heavy ions that are trapped near the equator. *Perraut et al*. [1982] with Geodetic Earth Orbiting Satellite (GEOS) 1 and 2 ULF wave and energetic particle data found that the waves that occurred at all *L* values inside the plasmasphere were predominant in the premidnight and dusk local times and were often associated with ~5–30 keV ring-like proton distribution functions. They suggest that the ring-like distributions lead to wave generation through nonresonant instabilities. *Horne et al*. [2000] concluded that the waves were generated by a cyclotron resonant instability by injected ring current ions having ring distributions. *Santolik et al*. [2002] using Cluster data noted that the emission lines did not match the local proton cyclotron frequency or its

harmonics and suggested that the waves may be generated at different locations (near the equator) and propagate to the point of observation. *Santolik et al*. [2004] noted that magnetosonic waves were detected 60% of the time for locations between 3.9 and 5 R_E and found the waves to be localized to within ~10° of the magnetic equator. The latter authors stated that the magnetosonic waves are the most intense, naturally occurring magnetic fluctuations in these locations and in the frequency range between the proton cyclotron and lower hybrid frequencies and thus may be very important for wave-particle interactions. *Meredith et al*. [2008] using CRRES plasma wave data noted that the intensity of the magnetosonic waves within the frequency range ~0.5 to 1.0 f_{LHR} (where f_{LHR} is the lower hybrid resonance frequency) increased with increasing geomagnetic activity, implying that the waves occur in intervals of enhanced convection and/or during substorms. Inside the plasmasphere the waves were detected only on the duskside, implying that $E < 30$ keV proton rings are the source of the waves. *Pokhotelov et al*. [2008] found this same local afternoon dependence for magnetosonic waves by using Cluster data.

Horne et al. [2007] showed that magnetosonic waves could accelerate electrons between ~10 keV and ~100 keV to relativistic energies via a Landau resonance and concluded that they might play an important role in radiation belt dynamics. *Meredith et al*. [2008] and *Thorne* [2010] demonstrated that the time for acceleration was ~1–2 days. *Bortnik and Thorne* [2010] have done test particle simulations of the scattering of energetic electrons interacting with magnetosonic waves and have confirmed the Landau resonance mechanism of *Horne et al*. [2007]. *Bortnik and Thorne* [2010] also mentioned that nonresonant transit time scattering by the waves may also be important.

It is the purpose of the present work to use ~ 1 year of Polar plasma wave data to do both statistical and detailed case studies of magnetosonic waves at and inside the plasmapause. Triaxial magnetic (*B*) wave high time resolution data will be used to identify all wave events, ensuring that the events used in the statistical studies are indeed magnetosonic waves. When uncontaminated wave electric field (*E*) data are available (this will be discussed in the Method of Analysis Section), this component will be shown in selected cases. It should be noted that this study will entail a 1996–1997 interval, which was a period of solar minimum [*Tsurutani et al*., 2011a]. Thus, one might expect some different results from previous statistical surveys, due to a lack of interplanetary coronal mass ejections during this phase of the solar cycle and thus a lack of major (*SYM-H* < -100 nT) magnetic storms [*Tsurutani et al*., 2006a, 2011a, 2011b]. The spatial (MLT, *L* value, and MLT), and geomagnetic activity (AE and SYM-H) dependences of the waves will be determined. High time resolution wave data will be used to determine the wave polarization and intensity as a function of distance from the presumed magnetic equatorial generation region and other detailed properties for particularly interesting case studies. Some surprising and unexplained results are obtained.

2. Method of Analyses

One year of Polar Plasma Wave Instrument (PWI) data [*Gurnett et al*., 1995] has been analyzed to study magnetosonic waves: 1 April 1996 to 4 April 1997. Only waves at and inside the plasmapause were included. Because there were instrumental problems with the electric field (*E*) measurements within the high-density plasmasphere (there were preamplifier oscillations, at times corrupting some of the measurements), these surveys will be conducted for only the magnetic field component (*B*) of the waves. At times when the instrument makes valid *E* measurements, some select examples will be shown. For the statistical surveys, the ~2 kHz bandwidth high-frequency waveform receiver (HFWR) covering the frequency range ~20 Hz to 2000 Hz, obtaining ~0.5 s snapshots every ~2 min interval overview data [*Santolik et al*., 2001], were used. The ~ 2 min interval is used as a basis for our statistical study and will hereby be called an "interval." If magnetosonic waves are detected during the interval, it will be called a wave "event."

There were 1013 Polar inbound and 1013 outbound crossings, or a total of 2026 passes during the approximate year of the study. Of these, there were 814 passes where the Polar HFWR wave data ~ 2 min overview plots were available. For each pass, there are many 2 min intervals and thereby many possible wave events. The plasmapause was identified by the electron plasma frequency characteristics in these plots. These 814 passes are the bases for statistical surveys that follow.

The ~2 min magnetosonic wave events were examined in detail. For every possible wave event, the high time resolution ~0.5 s plasma wave data (PWI 2 kHz HFWR data) [*Gurnett et al*., 1995] were plotted and hand inspected. The criteria used for identifying magnetosonic waves are that the waves were electromagnetic

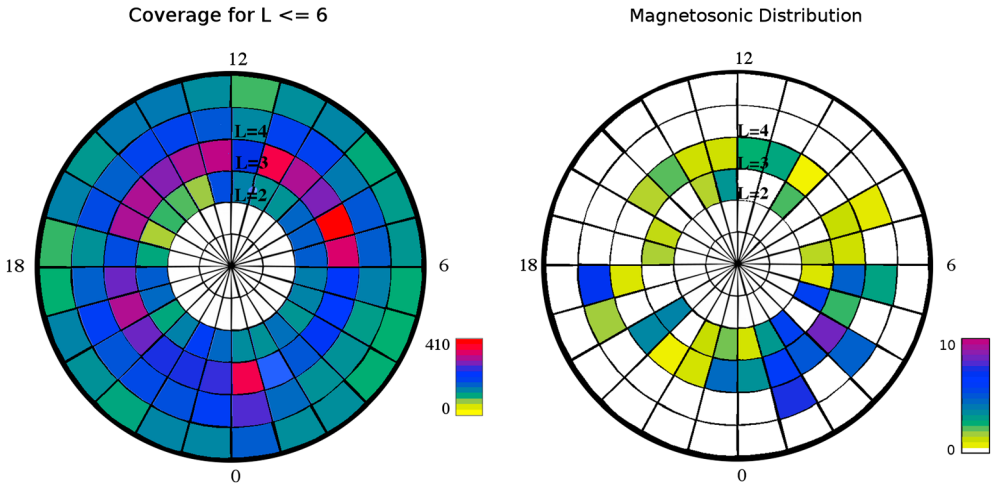

Figure 1. (left) The baseline coverage for the statistical survey and (right) percent occurrence of magnetosonic waves. Midnight is at the bottom and local dawn on the right. For Figure 1 (left), a color code gives the number of coverage intervals in that ΔL-ΔMLT range. For Figure 1 (right), the color code gives a normalized percent occurrence.

and the magnetic amplitudes were in the ambient magnetic field-aligned direction, B_0. In cases where the electric field components (E) were available and not contaminated, that was used as well. The E component should be large in a transverse direction to the ambient magnetic field B_0.

It was found that in many cases, both magnetosonic waves and a transverse electromagnetic wave mode (which appears to be the same as the plasmaspheric hiss identified in *Tsurutani et al*. [2011a, 2012]) were present at the same time. These two modes are easily distinguished from each other. The magnetosonic mode has field-aligned magnetic perturbations, whereas the transverse electromagnetic (EM) mode has magnetic perturbations orthogonal to B_0. For practical purposes, we will call the transverse mode plasmaspheric hiss. In all of these cases near the magnetic equator, the magnetosonic wave intensities were higher than that of the hiss. These events were used in the statistical survey part of the study. We feel that because the transverse EM waves were lower in amplitude than those of magnetosonic waves, this should not bias the results. The onset and cutoff times of the magnetosonic waves were noted and were used in our statistical analyses.

For all detailed wave analyses, the PWI 2 kHz HFWR three-axis B and three-axis E plots (when available) were used. Analyses were performed on these data using a minimum variance technique [*Sonnerup and Cahill*, 1967; *Smith and Tsurutani*, 1976] to determine wave polarization, direction of propagation, etc. The authors used single wave cycles for further detailed analyses.

3. Results

3.1. Statistical Studies

3.1.1. Location of Waves

Figure 1 (left) displays the coverage of the Polar spacecraft in L and MLT for the ~1 year interval. As previously mentioned, only passes where the PWI 2 kHz HFWR high time resolution data were available are used in our statistics. Noon is at the top, and dawn is at the right. The ΔL-ΔMLT bin resolution for the survey is $\Delta L = 1$ and ΔMLT = 1 h. The number of intervals (given in number of ~2 min intervals) per bin is given in the legend on the bottom right. In the figure, it is noted that the coverage from $L = 2$ to $L = 6$ and all MLTs is good.

Figure 1 (right) gives the L-MLT distribution for the magnetosonic waves. The scale is normalized percent occurrence (number of wave events divided by the total number of intervals for that bin). There are several outstanding features that can be noted from this distribution. The first is that the waves are present at all local times. There is a slight tendency for the waves to occur more frequently in the midnight-postmidnight sector (23 to 04 MLT) rather than in the premidnight sector. The peak occurrence frequency there is ~6–8%. The low-occurrence frequency is partly due to the highly eccentric Polar orbit. This point and others will be discussed further in a later section of the paper. A second important feature is that there were no waves detected from $L = 5$ to 6.

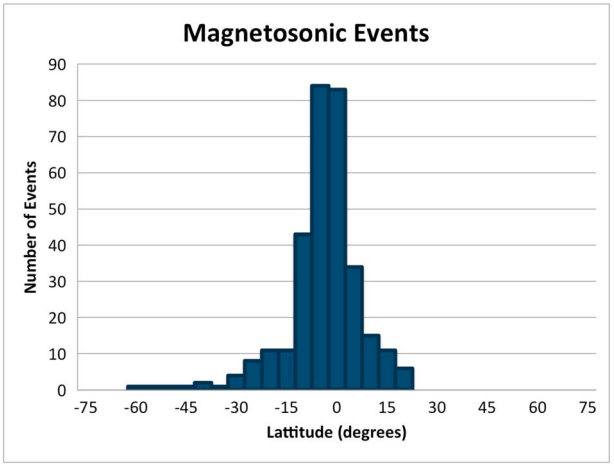

Figure 2. The latitudinal distribution of magnetosonic waves. The waves are located near the magnetic equator. However, they are also detected at latitudes away from the equator.

Figure 2 gives the magnetosonic wave latitudinal coverage (relative to the magnetic equator). The waves are principally detected at the magnetic equator, within ±5° of the magnetic equator. The half maximum occurred at ~±10°. This is consistent with the results of previously performed surveys. However, it is noted that waves were detected at latitudes as high as +20° and as low as −56°. For these extreme cases, the high-resolution data were double checked to ensure that these wave events indeed contained some "magnetosonic" components (there was often a mixture of transverse whistler mode hiss present as well). More will be stated about these particular wave features in a later section.

3.1.2. Wave Intensities

Figure 3 gives the magnetosonic wave power spectral densities (psds) as a function of latitude. The magnetic component units are in nT^2/Hz. It is noted that the peak magnetosonic wave psds are found to occur within ~±5°of the magnetic equator. The half values of the peaks are located at ~±10° latitude away from the equator. As previously mentioned, there are magnetosonic waves detected well off of the equator as well, but their psds are lower.

There are some exceptionally intense intervals noted in Figure 3. The peak magnetic psd of $\sim 4 \times 10^{-2}$ nT^2/Hz is noted at ~−2° latitude. However, this value occurred in only one measurement as indicated in the graph. The peak electric psd is at the equator with a value of ~2 $mV^2/m^2/Hz$ (for this example, the electric measurements were not corrupted). If one assumes a wave bandwidth of ~100 Hz, the peak magnetic wave amplitude measured from this study would be ~2.0 nT. The peak electric field amplitude would be ~14 mV/m. More will be stated about this event in the method of analysis section.

These peak wave psd events were relatively rare and were separated from the bulk of the other measurements. More typical peak wave psds are $\sim 5 \times 10^{-4}$ nT^2/Hz and $\sim 5 \times 10^{-1}$ $mV^2/m^2/Hz$ at the magnetic equator (the *E* power is not shown). Assuming a ~100 Hz bandwidth, this would correspond to $\sim 2 \times 10^{-1}$ nT and ~7 mV/m amplitudes, about an order of magnitude and a half order of magnitude lower, respectively.

The electric field component *E* is generally well above the noise level. The peak values are not so closely confined to the magnetic equator as the magnetic component of the waves. This has not been shown in order to save space.

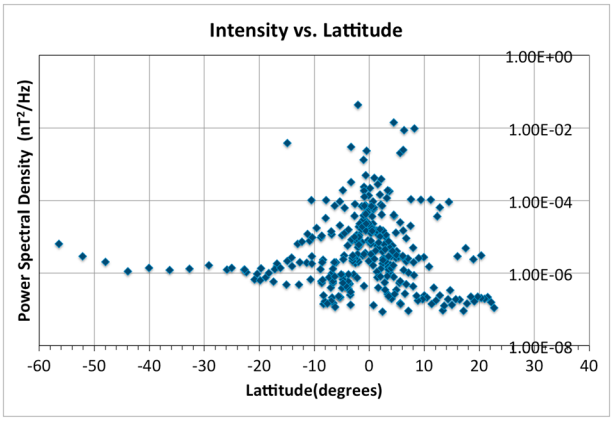

Figure 3. Magnetosonic wave magnetic (B_w) power spectral densities as a function of latitude. The peak magnetic value of $\sim 4 \times 10^{-2}$ nT^2/Hz is noted at ~−2° latitude. Assuming a wave bandwidth of ~100 Hz, the wave amplitude would be ~2 nT.

There are magnetosonic waves that are present in the $\sim 10^{-7}$ to 10^{-5} nT^2/Hz range outside of ±10° latitude. There is one event that goes from −10° to −56°. The wave psd values were more or less constant throughout this range, although a clear intensification as a function of latitude can be noted in the electric field component (not shown).

3.1.3. Wave Geomagnetic Activity Dependences

Figure 4 gives the background *SYM-H* distribution for all of the ~2 min intervals/events of the study (shown in black). The legend (number of events) is given on the right. The background SYM-H histogram

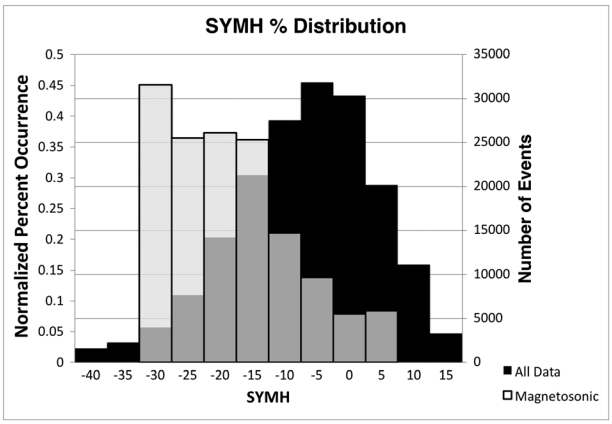

Figure 4. The *SYM-H* distribution of magnetosonic wave events (white) versus background (black). The black histogram is behind the white one, so the overlap is shown as grey. The black distribution has been truncated for ease of viewing.

was truncated at both ends for ease of viewing. The percentage magnetosonic wave events for each *SYM-H* bin are shown in white. The legend is given on the left. The black histogram is plotted behind the white histogram, so the former shows through as a grey color where they overlap. The average *SYM-H* for the interval of study was −10.1 nT and that for magnetosonic wave events −16.3 nT. It is clear that the two distributions are considerably different from each other. The magnetosonic waves are occurring during enhanced geomagnetic activity when the *SYM-H* values range from ~0 to −35 nT. Although these negative *SYM-H* values are not as large as *SYM-H* < −50 nT, the typical value used as a threshold for magnetic storms [*Gonzalez et al*., 1994], there must be considerable geomagnetic activity occurring, perhaps associated with high-speed solar wind streams [*Tsurutani et al*., 1995].

The format for Figure 5 is the same as that in Figure 4, except this figure illustrates the *AE* index dependences. The background *AE* shown in black are all ~2 min intervals/events used in the study. The scale giving the number of events is on the right. The magnetosonic wave events are given in white with the percent occurrence for each *AE* bin on the left. No time delays were taken into account for either gradient drifting ions or electrons. Magnetosonic wave events occurred during an *AE* range from 0 to 800 nT, with an average value of 233 nT. The distribution of *AE* for the magnetosonic waves is much different than the background *AE* distribution. It can be concluded from the figure that the wave events are generally occurring during substorms/magnetospheric convection events.

Although the preponderance of evidence (see section 1) is that these waves are generated by ~1–30 keV ions, it is unclear how waves might be generated in the dawn and noon sectors. More will be stated about this later.

Because the detection of magnetosonic waves depends on the location of the spacecraft in *L* and MLAT and the ongoing geomagnetic activity, the 22 MLT to 02 MLT and $\Delta L = 3$–4 region was reexamined using more restrictive conditions. The region was noted previously in the discussion of Figure 1 (right). In our more restrictive survey, only the $-5° \le$ MLAT $\le 5°$ region and various *AE* thresholds were studied. The results are given in Table 1.

The results of the restrictive survey show a significant difference in the magnetosonic wave occurrence frequency and local time distribution. It is now noted that for both *AE* > 300 nT and >400 nT, waves are present about half the time in the 23 ≤ MLT ≤ 24 range. Even more surprising, magnetosonic waves are almost never present in the premidnight 22 ≤ MLT ≤ 23 h and not at all in the postmidnight 01 ≤ MLT ≤ 02 h. However, it should be mentioned that the statistical significance is not high, as there are few intervals and wave events. One possible explanation for this observation is that substorms generally have all of the features that magnetic storms have: there are strong inward convection of the plasma sheet ions and electrons and thus heating of both

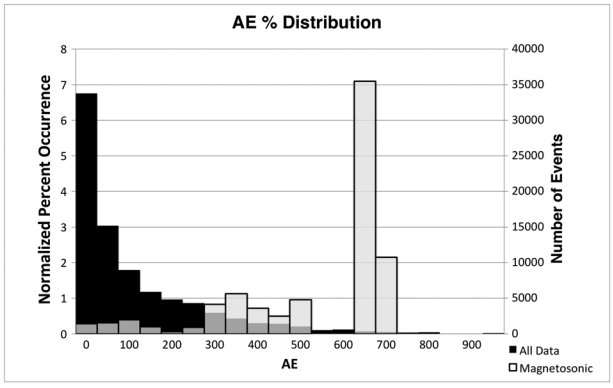

Figure 5. The *AE* distribution for magnetosonic waves (white) versus background (black). The grey tone is the black showing through the white histogram.

Table 1. The Percent Occurrence of Magnetosonic Waves for $\Delta L = 3$–4 and $-5° \le$ MLAT $\le 5°$ for a Variety of *AE* Thresholds

AE Threshold (nT)	22 to 23 MLT (%)	23 to 24 MLT (%)	00 to 01 MLT (%)	01 to 02 MLT (%)
>200	2	24	11	0
>300	0	147	12	0
> 400	0	46	18	0

particle species in the perpendicular (to the magnetic field) direction. However, substorm convection electric fields are generally more confined to the midnight sector [*Tsurutani and Smith*, 1974; *Tsurutani and Gonzalez*, 2006] and thus one might expect the magnetosonic waves to be as well.

3.2. Case Studies

3.2.1. Large-Magnitude Wave Event

We examine the case of very large wave amplitudes first, to illustrate an extreme case. The largest magnetosonic B_w amplitude event of Figure 3 will be studied in some detail. The event occurred at 0745 UT on 14 April 1996 at an *L* of 3.5, at 0022 MLT, and MLAT of −0.5°. The event occurred when *AE* was 624 nT and *SYM-H* was −33 nT. The *AE* and *SYM-H* indices were examined for several hours around the time of the wave event. It was found that *AE* was continuously high and fluctuating (the average for the hour was ~500 nT), and *SYM-H* was continuously negative with about the same value as listed above. This indicates that there was continuous geomagnetic activity going on. However, the solar wind speed was only $V_{sw} \sim 430$ km/s, and thus, this was clearly not associated with a coronal hole high-speed stream [*Tsurutani and Gonzalez*, 1987; *Tsurutani et al*., 2006a, 2006b; *Hajra et al*., 2013]. The detailed results are not shown to conserve space.

Figure 6 shows the magnetic (left) and electric (right) components of a ~0.5 s section of the waves in a field-aligned coordinate system (the *B*3 and *E*3 components are along B_0). Almost all of the wave magnetic fluctuations (bottom, left) are along B_0. What is particularly interesting is that the wave magnetic amplitude reaches a maximum value close to ~ ±1.0 nT. This was the largest wave amplitude detected during this study. The outer edge of the plasmapause was located at $L = 3.5$ during this pass. Thus, the waves shown in Figure 6 are located both at the plasmapause and the magnetic equator.

The above magnetic wave amplitude is reasonably consistent with the amplitude deduced from Figure 3, where a ~100 Hz bandwidth was assumed to derive an ~2.0 nT peak-to-peak amplitude. More will be stated about this later.

It should be noted that this is either the largest or one of the largest ELF wave magnetic magnitudes ever detected within the magnetosphere. As an example, outer zone chorus has peak magnetic intensities ~ 1 order of magnitude lower.

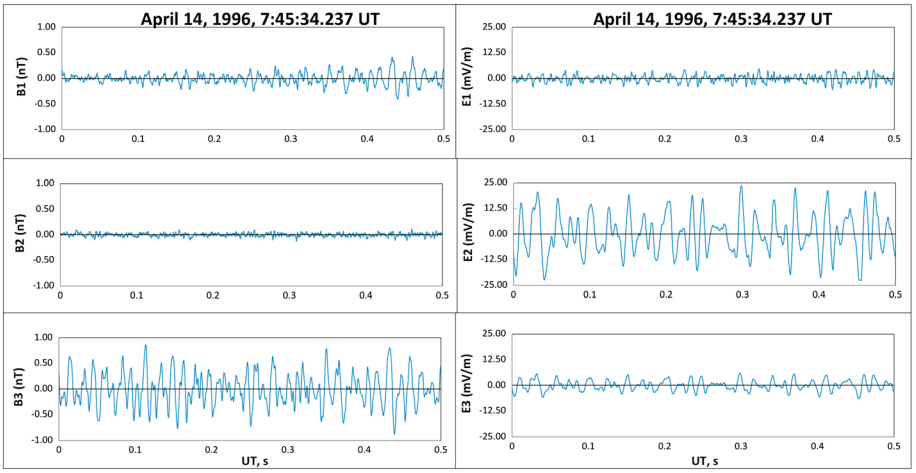

Figure 6. The (left) magnetic and (right) electric components of a magnetosonic wave event in field-aligned coordinates. In this system *B*3 and *E*3 are in the direction of the ambient magnetic field B_0. It is clear that almost all of the wave magnetic fluctuations are along B_0. The electric component waves (*E*2) are in a direction orthogonal to B_0. The wave is linearly polarized.

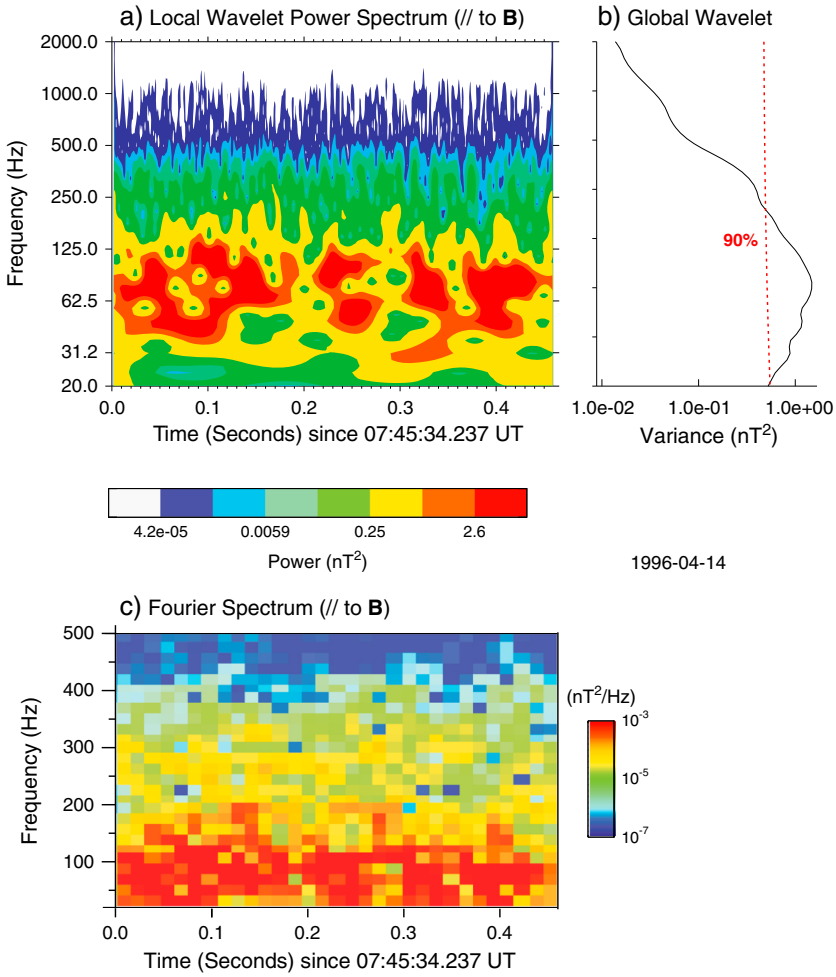

Figure 7. Wavelet analysis for the magnetosonic wave interval of Figure 6: (a) the local wavelet power spectrum for the magnetic component, (b) the global wavelet power spectrum, and (c) the Fourier spectrum of the same interval as Figures 7a and 7b.

The electric component of the wave is shown in field-aligned coordinates in the right-hand part of Figure 6. The wave electric amplitudes are almost solely in the E2 direction which is orthogonal to the ambient magnetic field direction, B_0. A remarkable feature of these waves is that the amplitudes almost reach ±25 mV/m.

Figure 7 shows a wavelet analysis of a portion of the B3 magnetic component of the magnetosonic waves of Figure 6. The wavelet plot is given in Figure 7a, the global wavelet power spectrum in Figure 7b, and the Fourier spectrum in Figure 7c. The frequency scale in Figure 7a is logarithmic, and the wavelet power/intensity is given in nT^2 [*Torrence and Compo*, 1998]. The Fourier spectral plot in Figure 7c has a linear frequency scale, and the power spectral density is given in nT^2/Hz. $|B_0|$ for this interval was 659 nT (measured by the onboard magnetometer), indicating a local proton cyclotron frequency of 10.1 Hz. What is clear from both the wavelet spectra and the fast Fourier transform spectra is that the wave power lies in a broad spectral range from ~30 to ~150 Hz. The peak psd in the waves is $>10^{-3}$ nT^2/Hz. For the E2 component (not shown), the power spectrum had intensities of ~1 mV^2/m^2Hz. These intense average values are generally consistent with the waveform results of Figure 6.

There is little or no evidence of proton cyclotron harmonics for this event. To try to resolve if there were cyclotron harmonics present, the 2 kHz mode receiver data, which has a maximum frequency resolution of 2.2 Hz, was analyzed. Cyclotron harmonics were not detected. To search for the proton cyclotron fundamental and first harmonic waves, the low-frequency waveform receiver 0 to 25 Hz data with a frequency resolution of 0.4 Hz were also studied. Neither the fundamental nor the first harmonic could be identified, although a rather broad band of electromagnetic waves at ~18 to 27 Hz (almost twice the

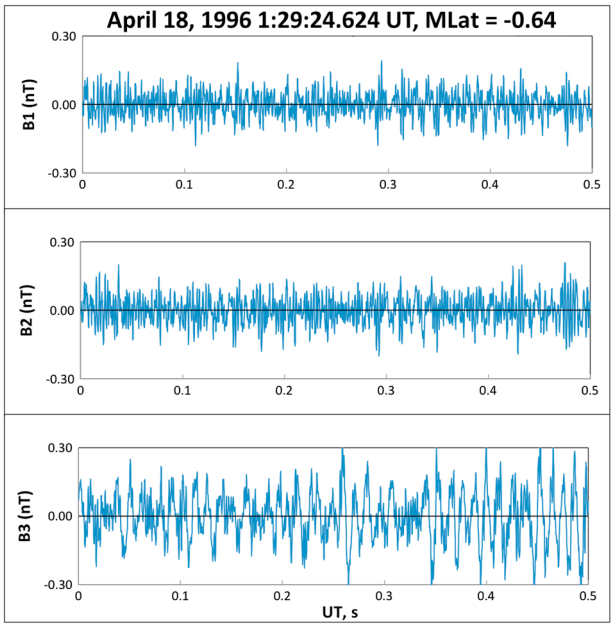

Figure 8. Format similar to Figure 6. Magnetosonic waves with superposed transverse electromagnetic waves near local noon at L = 2.6.

proton cyclotron frequency and greater) was observed in B3 with an amplitude of ~0.2 nT. The electric amplitude (in one of the perpendicular E components) was ~12 mV/m. This occurred approximately 4 s after the event shown in Figures 6 and 7. However, these waves were observed throughout the entire equatorial crossing from ~ 3° to −5°. The waves are most likely the unresolved low-frequency part of the magnetosonic waves observed at higher frequencies in Figures 6 and 7. The explanation for the lack of harmonic structures is beyond the scope of the paper and requires further theoretical investigations.

3.2.2. Evolution of Equatorial Magnetosonic Waves

Figure 8 shows a snapshot of a near-equatorial magnetosonic wave event (MLAT = −0.6°) which occurred near local noon (1208 MLT). This particular 0.5 s interval occurred at 0129:24 UT, 18 April 1996. *AE* was 675 nT, and *SYM-H* = −32 nT. The plasmapause was at $L = 2.9\ R_E$, and the wave event was at the outer edge of this structure. The electric component is not shown because of contamination. This snapshot was part of an extended wave event, starting from 0120:49 UT at a MLAT of −10.5° and lasting until 0153:01 UT where Polar was at 18.9° MLAT. There were continuous high time resolution data present throughout the interval.

In this figure there are clear magnetosonic fluctuations in the B3 (B_0 aligned) component. The amplitudes are as large as ± 0.4 nT. There are also fluctuations in the B1 and B2 (transverse) directions, but the frequencies are higher (different) than those in B3. The maximum amplitudes of B1 and B2 are ~0.2 nT, lower than those of B3. One possible interpretation is that this is a mixture of linearly polarized, field-aligned magnetosonic waves plus lower amplitude transverse electromagnetic waves (plasmaspheric hiss).

Figure 9 shows the waves at 0125:07 UT and MLAT = −5.3° for the same long-wave event as in Figure 8. The $B3$ field-aligned component has peak amplitudes of ±0.15–0.2 nT. The $B1$ and $B2$ peak components are ~ ±0.2 nT. Now the $B3$ amplitudes are smaller than those of the $B1$ and $B2$ amplitudes.

The many intermediate wave snapshots of this long-wave interval were not shown to save space. However, the general trend was illustrated in the above two figures, Figures 8 and 9. Near the magnetic equator, the largest wave amplitudes are in the field-aligned components, $B3$. These are the magnetosonic waves that have been reported in many previous studies. Further from the equator, the magnetosonic wave amplitudes decrease, and there are also higher-frequency transverse oscillations present. The decrease of the magnetosonic (longitudinal) waves with an increase of the transverse components is a gradual one. This happens as a function of distance away from the equator. This has not been shown explicitly to save space.

This general scenario of clear, large-amplitude magnetosonic waves at the magnetic equator, with decreasing amplitudes away from the equator, was a typical characteristic found in other magnetosonic wave events.

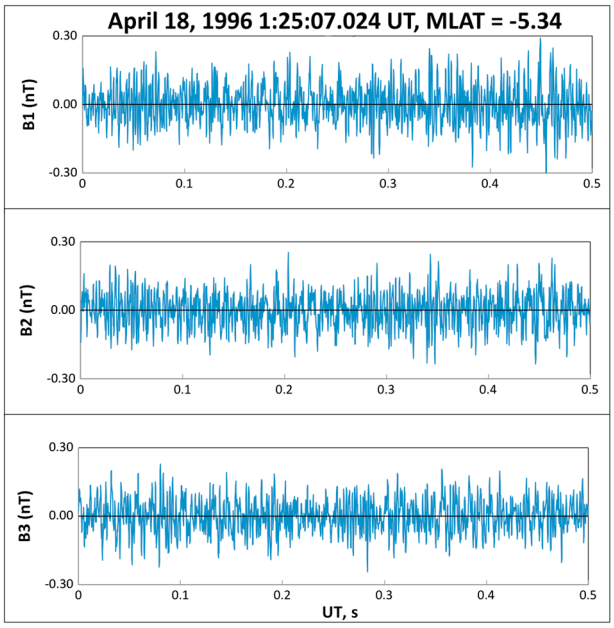

Figure 9. Format similar to that in Figure 6. The same wave event as in Figure 8 but earlier in time (0125:07 UT) and further from the equator (MLAT = −5.3°). The transverse wave amplitudes (*B*1 and *B*2) are slightly larger than the field-aligned component (*B*3).

The increase in amplitude of the transverse whistler mode waves with the decreasing magnetosonic wave amplitude was typical as well.

Figure 10 shows another example of dayside magnetosonic waves, at 1259:24 MLT (1031:21 UT) on 28 March 1997. The MLAT of the spacecraft was +0.4° and $L = 3.2$. The plasmapause was at 3.5 R_E, $AE = 47$ nT, and $SYM\text{-}H = +3$ nT. First, consider the three magnetic panels on Figure 10 (left). The dominant magnetic fluctuations occur in the *B*3 field-aligned component. The maximum amplitude is ~ ±0.3 nT. There are waves present in the two transverse components, *B*1 and *B*2, but much smaller in amplitude. Their maximum amplitudes are ~ ±0.01 to 0.02 nT. For the electric components of the waves, the maximum amplitudes are ~ ±0.3 mV/m in both the *E*1 and *E*2 (transverse) components. The *E*3 amplitudes are considerably less, perhaps ± 0.01 mV/m at the end of the interval. We interpret this as a superposition of magnetosonic waves plus smaller-amplitude transverse whistler mode waves.

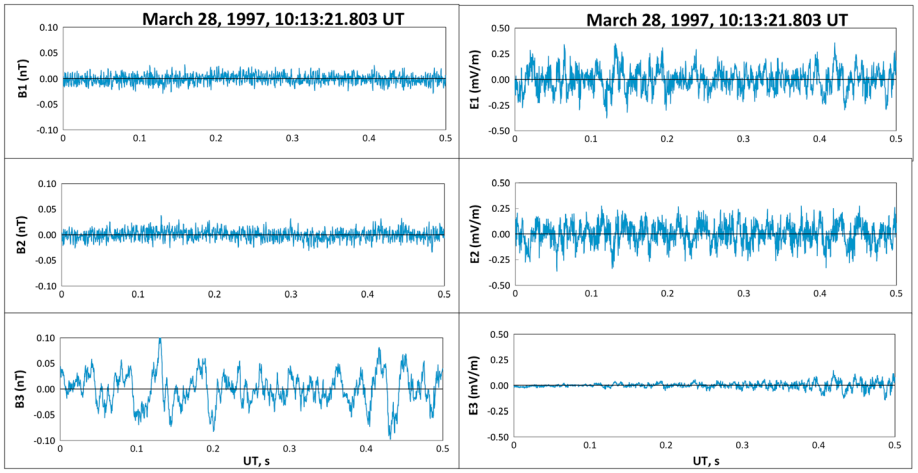

Figure 10. Magnetosonic waves at 1259:24 MLT on 28 March 1997. There are superposed transverse waves present as well.

4. Summary

The summary of the findings from the statistical studies and case studies of magnetosonic waves are given below:

1. Magnetosonic waves from a 1 year (1 April 1996 to 4 April 1997) statistical study indicated that the waves occurred at all local times and predominantly inside L = 4 (Figure 1). This limitation to L inside 4 is most probably associated with the spacecraft orbit. There was a slight increase in occurrence rate in the postmidnight sector, reaching a maximum of ~8% there.
2. Magnetosonic waves had peak occurrence rates at ~ ±5° relative to the magnetic equator, with half-peak rates at ±10° MLAT (Figure 2). Compressional linear magnetosonic components were detected as far as ~56° from the equator, however.
3. The highest magnetosonic wave intensities were detected within ±5° of the magnetic equator. The most intense wave event had $B_w = \sim \pm 1$ nT and $E_w = \sim \pm 25$ mV/m amplitudes. The magnetic component oscillations were magnetic field aligned, and the electric component oscillations were orthogonal to the magnetic field B_0, identifying these waves as linearly polarized (Figure 6).
4. For a more restrictive survey of a $22 \le \text{MLT} \le 02$, $3 \le L \le 4$, and $-5° \le \text{MLAT} \le 5°$ region, it was found that magnetosonic waves were present ~46% of the time for $AE > 300$ nT or 400 nT intervals for the $23 \le \text{MLT} \le 00$ region, and 0% for the $01 \le \text{MLT} \le 02$ region.
5. There was no evidence for proton cyclotron harmonics or other specific wave frequencies identified in the extreme event of Figure 6 (Figure 7). The psd spanned a frequency range of ~30 to ~150 Hz, whereas the local proton cyclotron frequency was ~10 Hz.
6. Magnetosonic waves statistically occur during relatively high geomagnetic activity intervals. They were found to be *SYM-H* (Figure 4) and *AE* (Figure 5) dependent. The waves were not detected during main phases of magnetic storms because storms were generally not present in the data set (the interval of study was during solar minimum). The most intense event (Figure 6) was detected at L = 3.5 at 0022 MLT and a MLAT of −0.5°. At the time the *AE* was 624 nT and *SYM-H* = −33 nT. This wave example occurred at the outer edge of the plasmapause.
7. The clearest magnetosonic wave signatures were noted at and near the magnetic equator. As the spacecraft moved away from the equator, the magnetosonic wave amplitudes decreased and transverse (orthogonal to B_0) electromagnetic wave amplitudes increased (Figures 8 and 9).
8. Magnetosonic waves were clearly present in the local daytime (Figures 8–10). Their characteristics seemed no different than those detected in the midnight sector. For the first case shown (Figures 8 and 9), there was moderate ring current (*SYM-H*) activity and high *AE* activity. However, for the second event (Figure 10), both *SYM-H* and *AE* were low.

5. Discussion and Conclusions

Some of the present results are consistent with the results of many other previous studies of magnetosonic waves: (1) the waves occurred during heightened geomagnetic (*AE*) activity, (2) the waves were primarily located close to the magnetic equator, and (3) the waves were observed at all local times. However, the present paper presents some differences as well. (4) The maximum normalized occurrence frequency was only ~8%, which is lower than any value of previously performed surveys. This low rate is partially due to the spacecraft orbit, where a good portion of its time was spent at high magnetic latitudes. It also may be partially due to the fact that the survey was done during solar minimum. When stronger restrictions were placed on both the satellite orbit and geomagnetic activity, waves were detected almost 50% of the time in the hour preceding midnight. (5) It was also noted that magnetosonic waves were detected at magnetic latitudes as large as 56°. This may be due to the reliance on the use of waveform data, which allowed tracking of magnetosonic waves to much lower amplitudes than previously done. The mixture of magnetosonic waves with plasmaspheric hiss may also have disguised the magnetosonic waves done in previous studies. The source of these high-latitude magnetosonic waves is, however, not well understood and needs further investigation.

Even with the lack of intense geomagnetic activity (e.g., magnetic storms), exceptionally large magnetosonic wave amplitudes ($B_w = \sim \pm 1$ nT, $E_w = \sim \pm 25$ mV/m) were detected. The reader might ask "Is this not a contradiction?" These waves were detected at local midnight (0022 MLT), at the magnetic equator (MLAT = −0.5°), at

the plasmapause ($L = 3.5$), and during a substorm ($AE = 624$ nT). We suggest that the spacecraft was perhaps at exactly the right place at the right time. Such intense waves may exist during all intense substorms without spacecraft in the correct position to make the measurements.

Different surveys of magnetosonic waves at and inside the plasmasphere have obtained different local time occurrence distributions. *Russell et al*. [1970] using OGO 3 data and *Kasahara et al*. [1994] using Akebono data found no obvious local time dependence for the waves. However, *Perraut et al*. [1982] using GEOS 2 data, *Pokhotelov et al*. [2008] using Cluster data, and *Meredith et al*. [2008] using CRESS data have found a dominance of magnetosonic wave occurrence on the duskside. *Meredith et al*. [2008] also surveyed magnetosonic waves outside the plasmasphere and found that they were more isotropically distributed there. However, those waves in the dawn sector were not accompanied by ions where the energies exceeded the Alfvén energy required for instability. It should be noted that the above-referenced surveys were conducted with different satellites having different orbits and were conducted during different phases of the solar cycle. Thus, one should not expect perfect agreement among them. The reader should also note that none of these surveys (this one included) have statistically significant results. That is because multiple measurements of the same wave event are not independent, and statistical tests should not be applied.

The popular mechanisms for the generation of magnetosonic waves near/inside the plasmapause are based on the nonresonant or resonant proton ring distribution instabilities [*Perraut et al*., 1982; *Boardsen et al*., 1992; *Horne et al*., 2000; *Pokhotelov et al*., 2008; *Meredith et al*., 2008]. In these mechanisms, protons are injected into the nightside magnetosphere during substorms or magnetic storms. The injection process will create proton temperature anisotropies ($T_{\perp}/T_{||} > 1$). Proton losses due to charge exchange with neutral hydrogen lead to ring distributions [*Fok et al*., 1995; *Jordanova et al*., 1996]. Consequently, proton ring distributions which have perpendicular proton temperatures greater than the parallel temperatures are produced. Such distributions possess free energy in the ring distribution as well as in the temperature anisotropy to drive the magnetosonic waves (and other wave modes as well).

The distribution of waves detected in the midnight sector (Figures 1, 6, and 7 and Table 1) at the equator during high *AE* values found in this study fits well with the above scenario proposed most recently by *Pokhotelov et al*. [2008] and *Meredith et al*. [2008]. It should be noted that storm time plasma sheet injections go deeper into the nightside magnetosphere where curvature and gradient drift of the ions will cause them to appear more on the duskside, whereas substorm injections are perhaps more localized and of shorter duration. For the postmidnight detection of magnetosonic waves, ion "banana orbits" and stagnation in postmidnight hours [*Chen et al*., 1994] are possible explanations for local generation of waves. Another possibility is that during active intervals, substorm occurrence may be shifted to local postmidnight hours, approximately midnight to ~04 MLT (A. Du, personal communication, 2013).

However, magnetosonic waves detected at other local times are still unexplained. Wave detection near local noon (Figures 8, 9, and 10) is particularly puzzling. This was noted by other surveys as well, although not as a particularly prominent feature. Our events were clearly magnetosonic mode waves so that one can be certain these events were not another wave mode masking themselves as magnetosonic waves (as previously speculated by other authors). There appears to be no obvious differences between those magnetosonic waves detected on the dayside from those in the midnight sector. One would of course have to have a different mechanism for the generation of those waves. It is noted that for the case in Figures 8 and 9, the *AE* activity was high. These waves could be due to nightside-injected protons that have drifted from midnight to noon. The postnoon wave event (Figure 10) occurred when the *AE* index was low. One possible explanation for this is that the dayside plasmasphere expanded outward (sunward) following convection events. The remnant energetic ions from previous substorm injections become engulfed by the high-density plasma leading to instability. Of course, more research on this topic is needed to determine if this speculation is correct or not.

In this study, a lack of proton cyclotron harmonic structure was noted. This is not presently explained. One of our referees has suggested several possibilities for our lack of proton cyclotron harmonic structure in the intense wave event: (a) very strong wave generation or (b) the waves might have an extended source region and the propagation of the usually banded structures have merged into a continuum or were subjected to mutual interactions. Following the suggestion, we have noted that at 0745: 34 UT there is evidence of H^+ ions with energies of 25 eV/e to 233 eV/e with pitch angles ~90°. We plan on studying these data in detail to

determine if an unusual proton distribution function can explain the lack of cyclotron harmonics or not. Another possibility is that the thermal spread of the ring distributions could possibly mask the harmonic structures.

Is it possible that even greater magnetosonic wave intensities exist but have not been detected yet? And if so, when would they occur, during substorms or storms? Current ideas are that strong magnetotail convection should lead to the greatest proton energization and greatest temperature anisotropies (ring kinetic energies). If this scenario is correct, then one would expect even greater wave intensities for these cases. Thus, one should look during intervals of superstorms when $SYM\text{-}H < -250$ nT [*Tsurutani et al*., 1992; *Echer et al*., 2008]. On the other hand, it is also possible that more intense substorm injections [*Tsurutani and Gonzalez*, 2006] may provide equally intense, but spatially limited, convection. This latter situation would support wave-particle interactions in the substorm/convection events associated with high-speed solar wind streams [*Tsurutani et al*., 2006a, 2006b] when relativistic electrons are accelerated. As of the present time, the greatest amplitude magnetosonic waves are ~ 1 order of magnitude more intense than chorus emissions (see *Tsurutani and Smith* [1977], *Santolik et al*. [2003], and *Tsurutani et al*. [2009, 2012] for chorus amplitudes). However, the same principle follows for chorus. They are generated by anisotropic electrons injected from the magnetotail into the magnetosphere during substorms and storms. We suggest examining outer zone chorus during intervals of strong substorms and/or superstorms to intercompare their intensities. The wave intensities during wave packets/subelements [*Santolik et al*., 2003; *Tsurutani et al*., 2013] should be examined carefully. It will be interesting to determine which wave mode has the highest amplitudes and under what conditions. Wave saturation may play a role. This is an exciting topic to investigate from a theoretical standpoint.

A new feature of magnetosonic waves was found. As the spacecraft went away from the magnetic equator during a magnetosonic wave event, the amplitude of the magnetosonic waves decreased while transverse wave amplitudes increased. Other similar cases were also noted. There are several possible scenarios that may explain these observations. The magnetosonic waves may lead to the scattering of electrons, and if the newly formed electron distribution is unstable, then transverse whistler mode waves may be generated. Further studies will be necessary to determine what the source of the transverse electromagnetic waves are.

Independent of the source of the waves, these transverse waves will also be important for wave-particle interactions, particularly for relativistic electrons. These transverse waves will propagate throughout the plasmasphere and will be a low-frequency source of plasmaspheric hiss, in addition to other mechanisms of plasmaspheric hiss as discussed by *Thorne et al*. [1979] and *Bortnik et al*. [2008].

6. Final Comments

In this paper, a case of a very large magnetosonic wave intensity event detected during an intense substorm has been emphasized. It was argued that the spacecraft was at exactly the right location at the right time, so in a way, there was a quite low probability for detecting this event. Why are these large intensities important? Our thought is that wave-particle interaction modelers should be using dynamical models with evolving particle clouds: from plasma sheet injections to azimuthal gradient and curvature drifts. The maximum wave amplitudes throughout the plasma clouds should be used instead of temporal and spatial averages to understand the effect of the waves on the particles. Temporal and spatial averages taken by satellite data surveys (like this one) are useful to understand the general processes of wave generation and propagation, but they are less useful for understanding the dynamics of the evolving plasma clouds.

Another wave mode, proton cyclotron (electromagnetic ion cyclotron or EMIC) waves, has also been suggested as a wave that can strongly interact with relativistic electrons. It should be mentioned to the reader that extremely large-amplitude (~ ±14 nT peak-to-peak) waves have been reported for one event [*Tsurutani et al*., 2003]. What is particularly interesting about this case is not only the unusually large amplitudes but also the location. These waves were not detected in the nightside or dusk equatorial plane as typically assumed for these waves but in the dayside polar cusp boundary layer. The authors have speculated that magnetic reconnection at the cusp has led to the generation of kinetic Alfvén waves which phase steepen, leading to ion perpendicular heating through the ponderomotive force. The anisotropic ions then generate the EMIC waves. Thus, we suggest that surveys be done for EMIC waves at large L on the dayside as well as for the interested researcher. The largest wave amplitudes would be of interest.

For the interested reader, it is noted that nonlinear Alfvén wave phase steepening [*Tsurutani et al*., 2002a], thermal ion perpendicular heating through the ponderomotive force [*Tsurutani et al*., 2002b; *Dasgupta et al*., 2003] generating diamagnetic dips in the interplanetary magnetic field, are common features in interplanetary space. The heated ions can at times generate EMIC waves [*Tsurutani et al*., 2002b], similar to the magnetospheric situation discussed above.

Acknowledgments

Portions of this research were performed at the Jet Propulsion Laboratory, California Institute of Technology under contract with NASA, and at the University of Iowa under JPL subcontract 1246597. O.S. acknowledges support from GACR205-10/2279 and LH11122. G.L.S. thanks the National Academy of Sciences, India, for the support under the NASI-Senior Scientist Platinum Jubilee Fellowship. We acknowledge NASA's CDAWeb for providing the TIMAS data used in this study. We thank the two referees for helpful comments/suggestions that have helped improve this paper.

Robert Lysak thanks Richard Horne and an anonymous reviewer for their assistance in evaluating this paper.

References

Andre, R., F. Lefeuvre, F. Simonet, and U. S. Inan (2002), A first approach to model the low-frequency wave activity in the plasmasphere, *Ann. Geophys.*, *20*, 981–996.

Boardsen, S. A., D. L. Gallagher, D. A. Gurnett, W. K. Peterson, and J. L. Green (1992), Funnel-shaped, low-frequency equatorial waves, *J. Geophys. Res.*, *97*(A10), 14,967–14,976.

Bortnik, J., and R. M. Thorne (2010), Transit time scattering of energetic electrons due to equatorially confined magnetosonic waves, *J. Geophys. Res.*, *115*, A07213, doi:10.1029/2010JA015283.

Bortnik, J., R. M. Thorne, and N. P. Meredith (2008), The unexpected origin of plasmaspheric hiss from discrete chorus emissions, *Nature*, *452*, 62–66, doi:10.1038/nature06741.

Chen, M. W., L. R. Lyons, and M. Schulz (1994), Simulations of phase space distributions of storm time proton ring current, *J. Geophys. Res.*, *99*, 5745–5759.

Dasgupta, B., B. T. Tsurutani, and M. S. Janaki (2003), A kinetic approach to the Ponderomotive Force, *Geophys. Res. Lett.*, *30*(21), 2128, doi:10.1029/2003GL017385.

Echer, E., W. D. Gonzalez, and B. T. Tsurutani (2008), Interplanetary conditions leading to superintense geomagnetic storms (Dst ≤ −250 nT) during solar cycle 23, *Geophys. Res. Lett.*, *35*, L06S03, doi:10.1029/2007GL031755.

Fok, M.-C., T. E. Moore, J. U. Kozyra, G. C. Ho, and D. C. Hamilton (1995), Three-dimensional ring current decay model, *J. Geophys. Res.*, *100*, 9619–9632.

Gonzalez, W. D., J. A. Joselyn, Y. Kamide, H. W. Kroehl, G. Rostoker, B. T. Tsurutani, and V. M. Vasyliunas (1994), What is a geomagnetic storm?, *J. Geophys. Res.*, *99*(A4), 5771–5792.

Gurnett, D. A. (1976), Plasma wave interactions with energetic ions near the magnetic equator, *J. Geophys. Res.*, *81*, 2765–2770.

Gurnett, D. A., et al. (1995), The polar plasma wave instrument, *Space Sci. Rev.*, *71*, 597–622, doi:10.1007/BF00751343.

Hajra, R., E. Echer, B. T. Tsurutani, and W. D. Gonzalez (2013), Characteristics and solar cycle dependences of high-intensity, long-duration, continuous AE activity (HILDCAA) events, relativistic electron predictors?, *J. Geophys. Res. Space Physics*, *118*, 5626–5638, doi:10.1002/jgra.50530.

Horne, R. B., G. V. Wheeler, H. St, and C. K. Alleyne (2000), Proton and electron heating by radially propagating fast magnetosonic waves, *J. Geophys. Res.*, *105*, 27,597–27,610.

Horne, R. B., R. M. Thorne, S. A. Glauert, N. P. Meredith, D. Pokhotelov, and O. Santolik (2007), Electron acceleration by fast magnetosonic waves, *Geophys. Res. Lett.*, *34*, L17107, doi:10.1029/2007GL030267.

Jordanova, V. K., L. M. Kistler, J. U. Kozyra, G. V. Khazanov, and A. F. Nagy (1996), Collisional losses of ring current ions, *J. Geophys. Res.*, *101*, 111–126.

Kasahara, Y., H. Kenmochi, and I. Kimura (1994), Propagation characteristics of the ELF emissions observed by the satellite Akebono in the magnetic equatorial region, *Radio Sci.*, *29*, 751–767.

Meredith, N. P., R. B. Horne, and R. R. Anderson (2008), Survey of magnetosonic waves and proton ring distributions in the Earth's inner magnetosphere, *J. Geophys. Res.*, *113*, A06213, doi:10.1029/2007JA012975.

Nemec, F., O. Santolik, K. Gereova, E. Macusova, Y. de Conchy, and N. Cornilleau-Wehrlin (2005), Initial results of a survey of equatorial noise emissions observed by the Cluster spacecraft, *Planet. Space Sci.*, *53*, 291–298.

Nemec, F., O. Santolik, K. Gereova, E. Macusova, H. Laakso, Y. de Conchy, M. Maksimovic, and N. Cornilleau-Wehrlin (2006), Equatorial noise: Statistical study of its localization and the derived number density, *Adv. Space Res.*, *37*, 610.

Nemec, F., O. Santolik, J. S. Pickett, Z. Hrbackova, and N. Cornilleau-Wehrlin (2013), Azimuthal directions of equatorial noise propagation determined using 10 years of data from the Cluster spacecraft, *J. Geophys. Res. Space Physics*, *118*, 7160, doi:10.1002/2013JA019373.

Olsen, R. C., S. D. Shawhan, D. L. Gallagher, J. L. Green, C. R. Chappell, and R. R. Anderson (1987), Plasma observations at the Earth's magnetic equator, *J. Geophys. Res.*, *92*(A3), 2385–2407.

Perraut, S., A. Roux, P. Robert, R. Gendrin, J.-A. Sauvaud, J.-M. Bosqued, G. Kremser, and A. Korth (1982), A systematic study of ULF waves above F_{H+} from GEOS 1 and 2 measurements and their relationships with proton ring distributions, *J. Geophys. Res.*, *87*, 6219–6236.

Pokhotelov, D., F. Lefeuvre, R. B. Horne, and N. Cornilleau-Wehrlin (2008), Survey of ELF-VLF plasma waves in outer radiation belt observed by Cluster STAFF-SA experiment, *Ann. Geophys.*, *26*, 3269–3277.

Russell, C. T., R. E. Holzer, and E. J. Smith (1970), OGO 3 observations of ELF noise in the magnetosphere 2. The nature of the equatorial noise, *J. Geophys. Res.*, *75*, 755–768.

Santolik, O., M. Parrot, L. R. O. Storey, J. Pickett, and D. A. Gurnett (2001), Propagation analysis of plasmaspheric hiss using Polar PWI measurements, *Geophys. Res. Lett.*, *28*, 1127–1130.

Santolik, O., J.S. Pickett, D. A. Gurnett, M. Maksimovic, and N. Cornilleau-Wehrlin (2002), Spatiotemporal variability and propagation of equatorial noise observed by Cluster, *J. Geophys. Res.*, *107*(A12), 1495, doi:10.1029/2001JA009159.

Santolik, O., D. A. Gurnett, J. S. Pickett, M. Parrot, and N. Cornilleau-Wehrlin (2003), Spatio-temporal structure of storm-time chorus, *J. Geophys. Res.*, *108*(A7), 1278, doi:10.1029/2002JA009791.

Santolik, O., F. Nemec, K. Gereova, E. Macusova, Y. de Conchy, and N. Cornilleau-Wehrlin (2004), System analysis of equatorial noise below the lower hybrid frequency, *Ann. Geophys.*, *22*, 2587.

Smith, E. J., and B. T. Tsurutani (1976), Magnetosheath lion roars, *J. Geophys. Res.*, *81*(13), 2261–2266.

Sonnerup, B. U., and L. J. Cahill Jr. (1967), Magnetopause structure and attitude from Explorer 12 observations, *J. Geophys. Res.*, *72*, 171–183.

Thorne, R. M. (2010), Radiation belt dynamics: The importance of wave-particle interactions, *Geophys. Res. Lett.*, *37*, L22107, doi:10.1029/2010GL044990.

Thorne, R. M., S. R. Church, and D. J. Gorney (1979), On the origin of plasmaspheric hiss: The importance of wave propagation during periods of substorm activity, *J. Geophys. Res.*, *84*, 5241–5247, doi:10.1029/JA084iA09p05241.

Torrence, C., and G. P. Compo (1998), A practical guide to wavelet analysis, *Bull. Am. Meteorol. Soc.*, *79*, 61, doi:10.1175/1520-0477.

Tsurutani, B. T., and E. J. Smith (1974), Postmidnight chorus: A substorm phenomenon, *J. Geophys. Res.*, *79*, 118–127.

Tsurutani, B. T., and E. J. Smith (1977), Two types of magnetospheric ELF chorus and their substorm dependences, *J. Geophys. Res.*, *82*, 5112–5128.

Tsurutani, B. T., and W. D. Gonzalez (1987), The cause of high intensity, long-duration continuous AE activity (HILDCAA): Interplanetary Alfvén wave trains, *Planet. Space Sci.*, *35*, 405–412.

Tsurutani, B. T., and W. D. Gonzalez (2006), A new perspective on the relationship between substorms and magnetic storms, in *Advances in Geosciences, Solar Terrestrial*, vol. 8, edited by M. Duldig et al., pp. 25–45, World Sci. Publ. Co., Hackensack, N. J.

Tsurutani, B. T., W. D. Gonzalez, F. Tang, and Y. T. Lee (1992), Great magnetic storms, *Geophys. Res. Lett.*, *19*, 73–76.

Tsurutani, B. T., W. D. Gonzalez, A. L. C. Gonzalez, F. Tang, J. K. Arballo, and M. Okada (1995), Interplanetary origin of geomagnetic activity in the declining phase of the solar cycle, *J. Geophys. Res.*, *100*(A11), 21,717–21,733.

Tsurutani, B.T., C. Galvan, J. K. Arballo, D. Winterhalter, R. Sakurai, and E. J. Smith (2002a), Relationship between discontinuities, magnetic holes, magnetic decreases, and nonlinear Alfvén waves: Ulysses observations over the solar poles, *Geophys. Res. Lett.*, *29*(11), 1528, doi:10.1029/2001GL013623.

Tsurutani, B. T., B. Dasgupta, C. Galvan, M. Neugebauer, G. S. Lakhina, J. K. Arballo, D. Winterhalter, B. E. Goldstein, and B. Buti (2002b), Phase-steepened Alfvén waves, proton perpendicular energization and the creation of magnetic holes and magnetic decreases: The ponderomotive force, *Geophys. Res. Lett.*, *29*(24), 2233, doi:10.1029/2002GL015652.

Tsurutani, B. T., B. Dasgupta, J. K. Arballo, G. S. Lakhina, and J. S. Pickett (2003), Magnetic field turbulence, electron heating, proton cyclotron waves, and the onsets of bipolar pulse (electron hole) events: A possible unifying scenario, *Nonlinear Proc. Geophys.*, *21*, 27–35.

Tsurutani, B. T., et al. (2006a), Corotating solar wind streams and recurrent geomagnetic activity: A review, *J. Geophys. Res.*, *111*, A07S01, doi:10.1029/2005JA011273.

Tsurutani, B. T., R. L. McPherron, W. D. Gonzalez, G. Lu, N. Gopalswamy, and F. L. Guarnieri (2006b), Magnetic storms caused by corotating solar wind streams, in *Recurrent Magnetic Storms: Corotating Solar Wind Streams*, vol. 167, edited by B. T. Tsurutani et al., pp. 1–17, AGU, Washington, D. C., doi:10.1029/167GM03.

Tsurutani, B. T., O. P. Verkhoglyadova, G. S. Lakhina, and S. Yagitani (2009), Properties of dayside outer zone chorus during HILDCAA events: Loss of energetic electrons, *J. Geophys. Res.*, *114*, A03207, doi:10.1029/2008JA013353.

Tsurutani, B. T., B. J. Falkowski, O. P. Verkhoglyadova, J. S. Pickett, O. Santolik, and G. S. Lakhina (2011a), Quasi-coherent chorus properties: 1. Implications for wave-particle interactions, *J. Geophys. Res.*, *116*, A09210, doi:10.1029/2010JA016237.

Tsurutani, B. T., E. Echer, and W. D. Gonzalez (2011b), The solar and interplanetary causes of the recent minimum in geomagnetic activity (MGA23): A combination of midlatitude small coronal holes, low IMF Bz variations, low solar wind speeds and low solar magnetic fields, *Ann. Geophys.*, *29*, 1–17, doi:10.5194/angeo-29-1-2011.

Tsurutani, B. T., B. J. Falkowski, O. P. Verkhoglyadova, J. S. Pickett, O. Santolik, and G. S. Lakhina (2012), Dayside ELF electromagnetic wave survey: A Polar statistical study of chorus and hiss, *J. Geophys. Res.*, *117*, A00L12, doi:10.1029/2011JA017180.

Tsurutani, B. T., G. S. Lakhina, and O. P. Verkhoglyadova (2013), Energetic electron (>10 keV) microburst precipitation, ~5–15 s X-ray pulsations, chorus, and wave-particle interactions: A review, *J. Geophys. Res. Space Physics*, *118*, 2296–2312, doi:10.1002/jgra.50264.